Oxidative switches in functioning of mammalian copper chaperone Cox17

Anastassia VORONOVA*, Wolfram MEYER-KLAUCKE†, Thomas MEYER‡, Annette ROMPEL‡, Bernt KREBS‡, Jekaterina KAZANTSEVA*, Rannar SILLARD* and Peep PALUMAA*[1]

*Department of Gene Technology, Tallinn Technical University, Akadeemia tee 15, 12618 Tallinn, Estonia, †EMBL-Hamburg Outstation, c/o DESY, Notkestrasse 85, 22603 Hamburg, Germany, and ‡Institut für Anorganische und Analytische Chemie, Westfälische Wilhelms-Universität Münster, Corrensstrasse 36, 48149 Münster, Germany

Cox17, a copper chaperone for cytochrome-*c* oxidase, is an essential and highly conserved protein in eukaryotic organisms. Yeast and mammalian Cox17 share six conserved cysteine residues, which are involved in complex redox reactions as well as in metal binding and transfer. Mammalian Cox17 exists in three oxidative states, each characterized by distinct metal-binding properties: fully reduced mammalian $Cox17_{0S\text{-}S}$ binds co-operatively to four Cu^+; $Cox17_{2S\text{-}S}$, with two disulfide bridges, binds to one of either Cu^+ or Zn^{2+}; and $Cox17_{3S\text{-}S}$, with three disulfide bridges, does not bind to any metal ions. The E_m (midpoint redox potential) values for two redox couples of Cox17, $Cox17_{3S\text{-}S} \leftrightarrow Cox17_{2S\text{-}S}$ (E_{m1}) and $Cox17_{2S\text{-}S} \leftrightarrow Cox17_{0S\text{-}S}$ (E_{m2}), were determined to be − 197 mV and − 340 mV respectively. The data indicate that an equilibrium exists in the cytosol between $Cox17_{0S\text{-}S}$ and $Cox17_{2S\text{-}S}$, which is slightly shifted towards $Cox17_{0S\text{-}S}$. In the IMS (mitochondrial intermembrane space), the equilibrium is shifted towards $Cox17_{2S\text{-}S}$, enabling retention of $Cox17_{2S\text{-}S}$ in the IMS and leading to the formation of a biologically competent form of the Cox17 protein, $Cox17_{2S\text{-}S}$, capable of copper transfer to the copper chaperone Sco1. XAS (X-ray absorption spectroscopy) determined that Cu_4Cox17 contains a Cu_4S_6-type copper–thiolate cluster, which may provide safe storage of an excess of copper ions.

Key words: Cox17, cytochrome-*c* oxidase copper chaperone, copper cluster, EXAFS, midpoint redox potential.

INTRODUCTION

CCO (cytochrome-*c* oxidase) is a terminal complex in the respiratory chain that transfers electrons from cytochrome-*c* to molecular oxygen [1]. Electron transfer by CCO is supported by two haems and three copper ions located in the binuclear Cu_A and mononuclear Cu_B sites respectively [2]. As copper ions are crucial for CCO functioning, *de novo* synthesized CCO subunits Cox I and Cox II have to be properly metallated. Research over the last decade has established that delivery and insertion of copper ions into CCO is an unexpectedly complicated process and occurs with the assistance of at least six copper chaperones: Cox17, Cox11, Sco1, Sco2, Cox19 and Cox23 [3]. On the basis of current information, Cox17 and Sco1 participate in the delivery of copper to the Cu_A site of CCO [4,5], whereas Cox11 delivers copper to the Cu_B site of CCO [6]. The roles of Cox19 and Cox23 in metallation of CCO are largely unknown.

Cox17, the first discovered copper chaperone for CCO, is a low-molecular-mass (7 kDa) protein that is essential for CCO assembly in yeast [7], as well as in mammalian cells [8]. Studies on yeast Cox17 demonstrate that the fully reduced form binds 2 [9] or 3 [10] mol of copper per mol of protein. Furthermore, luminescence and EXAFS studies have identified a solvent-shielded polycopper–thiolate cluster in fully reduced yeast CuCox17, which has been modelled by dicopper–tetrathiolate, tricopper–thiolate and even by hexacopper–thiolate clusters at the dimer interface [9,10]. However, the correct structure of this cluster in fully reduced yeast Cox17 is unknown.

Yeast Cox17 also exists in a partially oxidized form, of which the NMR structure is known [11]. Partially oxidized yeast Cox17 contains two disulfide bridges ($Cox17_{2S\text{-}S}$) and binds one Cu^+ ion, diagonally co-ordinated by two cysteine residues [11]. The fold of yeast $Cu_1Cox17_{2S\text{-}S}$ as well as apo-$Cox17_{2S\text{-}S}$ is composed from two short helixes interconnected with two disulfide bridges in the C-terminal region and from the N-terminal unstructured region [11]. The mammalian Cox17 has 30 % identity with yeast Cox17 and contains six absolutely conserved cysteine residues. Mammalian Cox17 also contains three histidine residues at the C-terminal region, which are absent from the yeast protein. ESI (electrospray ionization) MS has shown that the mammalian Cox17 can exist in three different redox states: fully reduced $Cox17_{0S\text{-}S}$, partially oxidized $Cox17_{2S\text{-}S}$ and fully oxidized $Cox17_{3S\text{-}S}$ protein [12]. Metal-binding studies confirmed that fully reduced mammalian $Cox17_{0S\text{-}S}$ co-operatively binds four Cu^+ into a solvent-shielded multinuclear copper–thiolate cluster, whereas partially oxidized $Cox17_{2S\text{-}S}$ binds one Cu^+ or Zn^{2+} ion, and fully oxidized $Cox17_{3S\text{-}S}$ cannot bind metals [12]. Mammalian $Cu_1Cox17_{2S\text{-}S}$ is thought to be structurally similar to yeast $Cu_1Cox17_{2S\text{-}S}$ [11]; however, the structure of the metal–thiolate cluster in mammalian Cu_4Cox17 is still not known.

Recently it was shown that partially reduced mammalian $Cox17_{2S\text{-}S}$ forms a specific metal-linked protein–protein complex with the copper chaperone Sco1 [13], indicating that the functional form of mammalian Cox17 in metallation of Sco1 may be $Cox17_{2S\text{-}S}$. Metallation of Sco1 takes place in the IMS (mitochondrial intermembrane space) where Cox17 is oxidized through a mechanism mediated by Mia40 proteins [14,15]. Therefore it is feasible that the functional metalloform of Cox17 in the IMS is $Cox17_{2S\text{-}S}$; however, obviously the two disulfide bridges in $Cox17_{2S\text{-}S}$ should be resistant to reduction at the redox potential values in IMS. It is known that the disulfide bonds in $Cox17_{2S\text{-}S}$ are fairly resistant to reduction [12]; however, the E_m (midpoint

Abbreviations used: CCO, cytochrome-*c* oxidase, DTT, dithiothreitol; DTT_{ox}, oxidized DTT; *E*, pH-corrected redox potential; *E′*, environmental redox potential; E_0, edge energy; E'_0, standard redox potential; E_a, activation energy; E_F, Fermi energy; E_m, midpoint redox potential; ESI, electrospray ionization; GFP, green fluorescent protein; IMS, mitochondrial intermembrane space; K, electron wave vector; MALDI, matrix-assisted laser-desorption ionization; MM, mitochondrial matrix; MT, metallothionein; PAMO, peptidylglycine α-amidating mono-oxygenase; RP-HPLC, reverse-phase HPLC; TCEP, tris(2-carboxyethyl)phosphine hydrochloride; TFA, trifluoroacetic acid; TOF, time-of-flight; XANES, X-ray absorption near edge structure; XAS, X-ray absorption spectroscopy.

[1] To whom correspondence should be addressed (email peepp@staff.ttu.ee).

redox potential) values for redox transitions between the different redox forms of Cox17 are unknown. There are also no direct data about the redox potential values in the IMS; however, by using redox-sensitive GFP (green fluorescent protein)-sensor proteins it has been estimated that the redox potential in mitochondrial matrix, as well as in the cytoplasm of plant and animal cells, is highly reducing ($E_m = -320$ and -360 mV respectively) [16–18] and only extremely stabile disulfide bonds might withstand these conditions.

The aim of the present study was to determine the E_m values between the two redox pairs of Cox17: $Cox17_{0S\text{-}S} \leftrightarrow Cox17_{2S\text{-}S}$ and $Cox17_{2S\text{-}S} \leftrightarrow Cox17_{3S\text{-}S}$. Comparison of obtained E_m values of the two Cox17 redox couples with cellular redox potentials enabled us to estimate the positions of the redox equilibria of Cox17 in different cellular compartments. We also characterized the structure of the metal-binding motif in fully reduced Cu_4Cox17 by EXAFS, which demonstrated the presence of a Cu_4S_6-type of metal thiolate cluster in Cu_4Cox17.

EXPERIMENTAL

Materials

Porcine Cox17 was isolated from porcine intestine as an apoprotein containing three disulfide bridges ($Cox17_{3S\text{-}S}$) and purified as described in [12]. Recombinant human apo-$Cox17_{3S\text{-}S}$ was expressed and purified as described in [19]. DTT_{ox} (oxidized dithiothrietol) was synthesized from reduced DTT according to the protocol described in [20]. Tris base and Hepes were both ultrapure MB (molecular biology) grade from USB (United States Biochemical) Corporation, other reagents of analytical grade were from Sigma–Aldrich.

Reduction of $Cox17_{3S\text{-}S}$ with DTT

Fully oxidized human recombinant $Cox17_{3S\text{-}S}$ (5 μM) was incubated in argon-saturated 20 mM Tris/HCl and 100 mM NaCl buffer, pH 7.6, containing 2, 5 or 10 mM DTT as a reducing agent. Separate reaction mixtures were incubated at temperatures of 35, 47 and 55 °C. At various time points, an aliquot from the reaction mixture was applied to the RP (reverse-phase)-HPLC column Lichrosorb RP8 (4 mm × 30 mm, bead size 7 μm) and analysed using an acidic solvent system, which stopped the reduction of $Cox17_{3S\text{-}S}$. Buffer A was 0.1 % TFA (trifluoroacetic acid) in water, buffer B was 0.1 % TFA in 95 % acetonitrile, and a gradient of 50–80 % buffer B over 5 column vol. was used. $Cox17_{2S\text{-}S}$ and $Cox17_{0S\text{-}S}$ eluted between 64.8–66.4 % and 65.6–68.7 % buffer B respectively. RP-HPLC chromatography was conducted on the Äkta™ Explorer chromatography system (Amersham Biosciences), and data were analysed for peak areas using Unicorn software (Amersham Biosciences). Decrease of the $Cox17_{2S\text{-}S}$ peak area was fitted using the equation of exponential decay, and first-order kinetic constants were calculated.

The activation energy (E_a) for $Cox17_{2S\text{-}S}$ reduction with 5 mM DTT was calculated from kinetic data at different temperatures using the Arrhenius equation:

$$\log k = -\frac{E_a}{2.3 \cdot RT} + \log A \quad (1)$$

where k is rate constant, R is gas constant (8.315 JK^{-1}), T is the absolute temperature and A is the pre-exponential factor.

Determination of redox potentials for Cox17 pairs

Fully oxidized human recombinant $Cox17_{3S\text{-}S}$ was incubated in degassed 20 mM Tris/HCl or Hepes and 100 mM NaCl, pH 7.6, containing various ratios of GSH/GSSG ([GSH] + 2[GSSG] = 5 mM) or DTT/DTT_{ox} ([DTT] + [DTT_{ox}] = 5 mM) as redox buffers. The redox potential of the buffer was adjusted by varying the ratio of the reduced and oxidized forms of GSH and DTT, and corresponding redox potentials have been calculated from the following Nernst equations:

$$E' = E'_0(\mathrm{GSH}) - (RT/nF)\ln\frac{[\mathrm{GSH}]^2}{[\mathrm{GSSG}]} \quad (2)$$

$$E' = E'_0(\mathrm{DTT}) - (RT/nF)\ln\frac{[\mathrm{DTT}]}{[\mathrm{DTT_{ox}}]} \quad (3)$$

where E'_0 is standard redox potential; E'_0 (GSH) = −0.24 V (pH 7.0 and 25 °C) [21], E'_0 (DTT) = −0.323 V (pH 7.0 and 30 °C) [22], R is the gas constant (8.315 J · K^{-1}), T is the absolute temperature, n is the number of transferred electrons, and F is the Faraday constant (9.649 × 10^4 C · mol^{-1}). E'_0 (GSH) and E'_0 (DTT) values have been recalculated for 37 °C by using eqns (2) and (3) and for pH 7.6 by using the following equation:

$$E_{pH} = E'_0 + (\mathrm{pH} - \mathrm{pH_0}) \times ({}^{\Delta E}/_{\Delta \mathrm{pH}}) \quad (4)$$

For the determination of different redox states of Cox17 in GSH-based redox buffers, fully oxidized $Cox17_{3S\text{-}S}$ (3 μM) was incubated at 37 °C for 75 min with the GSH/GSSG redox pairs, and the reaction was stopped by the addition of 25 mM iodoacetamide. The reaction mixture was incubated further for 60 min at 25 °C in the dark and protein adducts were identified by MALDI (matrix-assisted laser-desorption ionization)–TOF (time-of-flight) MS on the Voyager STR (Applied Biosystems) using 10 mg/ml sinapinic acid matrix in 50 % acetonitrile/0.1 % TFA. Mass spectra were acquired in reflector mode by using the following instrument parameters: acceleration voltage 2500 V, delay time 350 ns and low mass gate 1000 Da. On average, 30 laser shots were applied per sample, and the results obtained were analysed using the Data Explorer software (Applied Biosystems).

Equilibrium ratios of Cox17 redox forms in DTT-based redox buffers have been determined after 240 min of incubation of $Cox17_{3S\text{-}S}$ (5 μM) at 37 °C in DTT/DTT_{ox} redox buffers by RP-HPLC as described above. E_m values of $Cox17_{3S\text{-}S} \leftrightarrow Cox17_{2S\text{-}S}$ and $Cox17_{2S\text{-}S} \leftrightarrow Cox17_{0S\text{-}S}$ pairs were determined by fitting the dependence of $[Cox17]_{red}/[Cox17]_{ox}$ to the E' with the following equation [17]:

$$y = y_0 + \frac{A^*}{1 + e^{(x_0 - x)/13}} \quad (5)$$

where y is $[Cox17]_{red}/[Cox17]_{ox}$; x is the E'; y_0 and A^* are constants and x_0 is E_m. Fittings were performed using the program KyPlot (version 2.0 beta 15; KyensLab).

Air oxidation of fully reduced Cox17

Fully oxidized human recombinant $Cox17_{3S\text{-}S}$ (20 μM) was reduced for 3 h in argon-saturated 20 mM Tris/HCl and 100 mM NaCl buffer, pH 7.6, containing 5 mM DTT. Fully reduced $Cox17_{0S\text{-}S}$ was desalted using the HiTRAP™ Desalting (5 ml) column (Amersham Biosciences) into argon-saturated 20 mM Tris/HCl and 100 mM NaCl buffer, pH 7.6. Aliquots of desalted $Cox17_{0S\text{-}S}$ were mixed directly with $ZnCl_2$ dissolved in air-saturated 20 mM Tris/HCl and 100 mM NaCl buffer, pH 7.6, to a final metal concentration of 3 or 14 μM. For the negative control, air-saturated Tris/HCl buffer was added to $Cox17_{0S\text{-}S}$. Reaction mixtures were stopped at different time points through application to the RP-HPLC Lichrosorb RP8 column and analysed using an acidic solvent system as described above.

Analysis of Cox17 redox state in recombinant bacteria

The recombinant *Escherichia coli* strains BL21pLysS(DE3) and Origami™(DE3) (Novagen) carrying the Cox17 expression plasmid (pET11cCox17) were grown and induced as described in [19]. Harvested cells were stored at −80 °C. For protein expression analysis, the cells were lysed by thawing, and the cell lysate obtained was diluted 1:10 with a 20 mM Hepes and 100 mM NaCl, pH 7.6, buffer and allowed to react with 25 mM iodoacetamide for 1 h in the dark. The reaction products were analysed by MALDI MS as described above.

Preparation of Cu_4Cox17

To give a 75 μM solution, 2 mg of freeze-dried porcine $Cox17_{3S\text{-}S}$ was dissolved in argon-saturated 20 mM ammonium acetate, pH 7.5. The solution was reduced for 45 min at 55 °C with 0.25 mM DTT and 1.0 mM TCEP [tris(2-carboxyethyl)phosphine hydrochloride]. Four equivalents of the Cu(I)–DTT complex were added to the fully reduced protein, and the sample was concentrated by ultrafiltration through a 1 kDa cut-off membrane (Millipore) to the final 1 mM protein concentration. Cu(I)–DTT complex was prepared by dissolving copper(II) acetate in argon-saturated 20 mM ammonium acetate, pH 7.6, in the presence of 2 mM DTT. An ESI-MS spectrum from the concentrated sample was taken after a 100-fold dilution of the probe with 20 mM ammonium acetate, pH 7.6, containing 0.3 mM DTT. Prior to XAS (X-ray absorption spectroscopy), 20 % of degassed glycerol was added to the sample. Sample holders were filled under argon and shock-frozen in ethanol/solid CO_2 before cooling down with liquid nitrogen. Composition of the samples was tested by ESI TOF MS on an Ettan™ instrument (Amersham Biosciences), and copper content was determined by atomic absorption spectrometry on a PerkinElmer 3100 machine.

XAS studies

EXAFS probes of porcine Cu_4Cox17 were loaded under argon into 1-mm-thick plastic holders with Kapton windows and shock-frozen in ethanol/dry ice before cooling down with liquid nitrogen. XAS measurements were carried out at the EMBL (European Molecular Biology Laboratory) EXAFS beamline (D2) at DESY (Deutsches Elektronen Synchrotron) with the DORIS storage ring operating at 4.5 GeV. The ring currents ranged from 90 to 150 mA. The beam is diffracted by a temperature-controlled double crystal monochromator with two Si(111) crystals, and harmonic rejection is accomplished by detuning the first monochromator crystal to approx. 60 % of its peak intensity and a focusing mirror with a cut-off energy of above 21.5 keV. The monochromator angle was calibrated to an absolute energy scale by Bragg reflections from a static Si(220) crystal recorded simultaneously with the spectra [23]. To increase the dynamic order, the samples were kept at 20 K in a cryostat during the measurements. Fluorescence data were collected by a 13-element germanium detector (Canberra) [24]. The measured energy ranged from 250 eV below the Cu-K absorption edge (8979 eV) to 1000 eV above the Cu-K edge. The energy range of the spectra is by far longer than the ones presented in previous publications on copper proteins containing copper–thiolate clusters [25,26]. This was possible since our preparations did not contain any zinc and thus a longer energy range was available for data collection.

The data file for measurements was optimized in the step width with a continuously increasing number of data points per eV, starting with 0.5 data points per eV at high energies and reaching 2.4 data points per eV at the absorption edge. For data evaluation, the EMBL EXAFS program package EXPROG was used, and data evaluation analysis was carried out with the program CHAOS [28]. Overall, data from ten scans were used for data analysis, while the spectra derived from nine detector elements were taken into account. The experimental EXAFS spectra were compared with theoretical simulations obtained by the program EXCURV98 9.27 (CLRC Daresbury Laboratory, Warrington, U.K.) with curved-wave theory, von Barth/Hedin-Lundqvist phases and amplitude functions. The edge energy $E_0 = 8990$ eV was adjusted at the beginning of the refinement in order to bring the experiments and the simulations on the same scale. A fixed amplitude factor of 1.00 was used. The $\mathbf{k}^3$ weighted full spectra (where $\mathbf{k}$ is the electron wave vector) were simulated by varying the atom types and the coordination numbers (as integers) and iteratively refining the distance (R) and the Debye-Waller factor ($2\sigma^2$) for each atomic shell. The quality of the fit obtained was assessed by the goodness of fit function:

$$\varepsilon^2 = 1/(N_{\text{ind}} - p)(N_{\text{ind}}/N) \sum_i^N w_i \left[\chi_i^{\text{exp}}(k) - \chi_i^{th}(k)\right]^2 \quad (6)$$

where N_{ind} is the number of independent data points ($N_{\text{ind}} = 2\Delta k \Delta r/\pi$), p is the number of parameters, N is the number of data points and w is the weight of the spectrum. Quality of fit was also assessed by R_{exafs}-factor as defined within EXCURV 9.27:

$$R_{\text{exafs}} = \sum_i^N 1/\sigma\left[\left|\chi_i^{\text{exp}}(k) - \chi_i^{th}(k)\right|\right] \times 100 \quad (7)$$

New shells of scatterers introduced in the simulations have been maintained when their contribution increased the quality of fit as estimated by the goodness of fit criterion.

The theoretical calculation of the EXAFS spectra according to the crystallographic data for two copper-sulfur clusters, Cu_4S_6 [30] and Cu_5S_6 [31], was executed using the EXCURV92 tool of the Cerius^2 program package (Molecular Simulations) with the theoretical calculated phase and amplitude functions. Crystallographic data for these clusters were obtained from the Cambridge Structural Data Bank where they were denoted as HARFOV and CIRHEQ respectively.

RESULTS

E_m values for Cox17 redox pairs

In GSH/GSSG redox buffers, the equilibrium between $Cox17_{3S\text{-}S}$ and $Cox17_{2S\text{-}S}$ was reached in minutes, and formation of fully reduced $Cox17_{0S\text{-}S}$ was not observed even after prolonged incubation of $Cox17_{3S\text{-}S}$ with 5 mM GSH. However, in addition to the major $Cox17_{3S\text{-}S}$ and $Cox17_{2S\text{-}S}$ forms, the GSH–$Cox17_{2S\text{-}S}$ adduct was also detected by MALDI MS, and its content was dependent on the redox potential of the environment. Moreover, a minor GSH_2–$Cox17_{2S\text{-}S}$ adduct was also detected at high partial ratios of GSSG. Equilibrium ratios of $Cox17_{3S\text{-}S}$, $Cox17_{2S\text{-}S}$ and the GSH–$Cox17_{2S\text{-}S}$ adduct in GSH/GSSG redox buffers are presented in Figure 1(A). Fitting of equilibrium ratios for $Cox17_{3S\text{-}S}/Cox17_{2S\text{-}S}$ against E' according to eqn (5) yielded an E_{m1} of -197 ± 4 mV (pH 7.6, 37 °C). Further reduction of $Cox17_{2S\text{-}S}$ could be achieved by increasing the concentration of GSH; however, this complicated the reaction product detection by MALDI MS owing to the increasing concentrations of alkylating agent. Alternatively, a more powerful reducing reagent such as DTT could be used effectively for further reduction of $Cox17_{2S\text{-}S}$ [12].

Incubation of $Cox17_{3S\text{-}S}$ with millimolar concentrations of DTT led to an almost instantaneous formation of $Cox17_{2S\text{-}S}$ and a slow

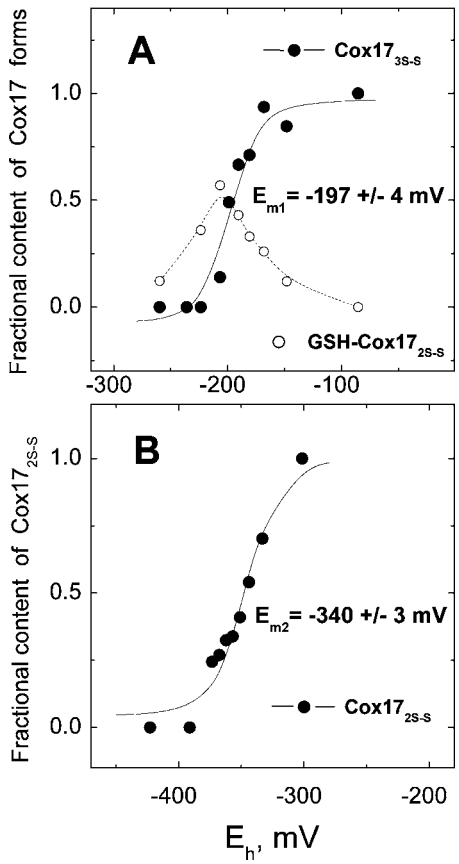

Figure 1 Determination of redox midpoint potentials of $Cox17_{3S-S} \leftrightarrow Cox17_{2S-S}$ (A) and $Cox17_{2S-S} \leftrightarrow Cox17_{0S-S}$ (B) couples

(**A**) Fractional content of $Cox17_{3S-S}$ (●) and of GSH–$Cox17_{2S-S}$ adduct (○) at different E' values generated by the GSH/GSSG couple. Continuous line, fitted curve with $E_{m1} = -197$ mV. (**B**) Fractional content of $Cox17_{2S-S}$ (-●-) at different E' values generated by DTT/DTT_{ox} couple. Continuous line, fitted curve with $E_{m2} = -340$ mV. For more details see the Experimental section.

formation of $Cox17_{0S-S}$ according to a first-order rate law. Reaction kinetic curves at different concentrations of DTT and temperature-dependence for Cox17 reduction at 5 mM DTT are presented in Figure 2. Using the Arrhenius equation (1) yielded an E_a of -60 kJ/mol for reduction of $Cox17_{2S-S}$ with 5 mM DTT (Figure 2, inset). Incubation of $Cox17_{3S-S}$ in DTT/DTT_{ox} redox buffers occurred with similar kinetics; however, at higher ratios of DTT_{ox}, reduction was incomplete and dependent on the percentage of DTT_{ox} in the reaction buffer. Equilibrium ratios of $Cox17_{2S-S}$ and $Cox17_{0S-S}$ in DTT/DTT_{ox} redox buffers determined after 3 h of incubation at 37 °C are presented in Figure 1(B). Fitting of these results according to eqn (5) yielded an E_m for $Cox17_{2S-S}$/$Cox17_{0S-S}$ pair equal to $E_{m2} = -340$ mV (pH 7.6, 37 °C).

Air oxidation of fully reduced Cox17

Fully reduced $Cox17_{0S-S}$ can bind up to two Zn^{2+}. To test whether metal binding protects $Cox17_{0S-S}$ from air oxidation we studied the effect of Zn^{2+} on air oxidation of $Cox17_{0S-S}$ by using HPLC, as described above. Zn^{2+} had an inhibitory effect on air oxidation of apo-$Cox17_{0S-S}$ even at a 3 μM metal concentration (inhibition of the rate of oxidation by 40%). Addition of 14 μM Zn^{2+} inhibited oxidation of Cox17 by 80% (results not shown).

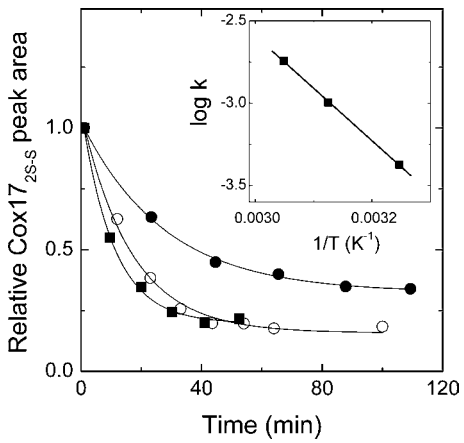

Figure 2 Kinetics of Cox17 reduction with DTT monitored by RP-HPLC

Kinetic curves of reduction at 47 °C at the following concentrations of DTT: 2 mM (●), 5 mM (○) and 10 mM (■). Inset: Arrhenius plot for reduction of $Cox17_{2S-S}$ with 5 mM DTT at 35 °C, 47 °C and 55 °C. Calculated activation energy is $E_a = -60$ kJ/mol.

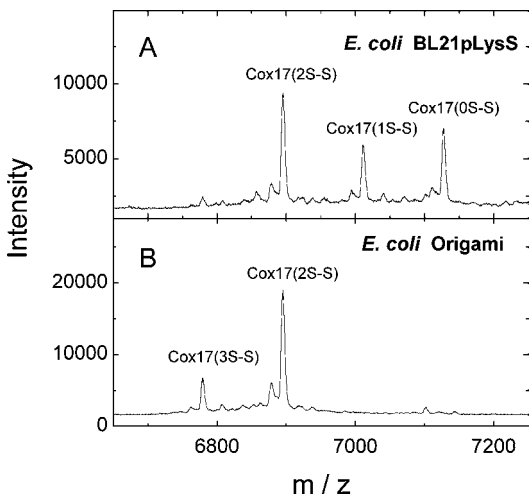

Figure 3 MALDI MS analysis of redox forms of recombinant Cox17 in *E. coli* strains

(**A**) BL21pLysS(DE3) strain; (**B**) Origami™(DE3) strain, which is deficient in *trxB* and *gor* genes and has a more oxidative cytosolic environment. A molecular mass of 7119.9 Da was assigned to $Cox17_{0S-S}$ with six carbamidomethyl groups attached; a molecular mass of 7005.9 Da was assigned to $Cox17_{1S-S}$ alkylated with four carbamidomethyl groups; a molecular mass of 6891.9 Da was assigned to $Cox17_{2S-S}$ alkylated with two carbamidomethyl groups; a molecular mass of 6777.9 Da was assigned to $Cox17_{3S-S}$. For more details see the Experimental section.

Cox17 redox state in recombinant bacteria

Protein expression analysis from the recombinant *E. coli* strains BL21pLysS(DE3) and Origami™(DE3) carrying the Cox17 expression plasmid (pET11cCox17) demonstrated that, in bacteria with an unaltered cellular redox environment, Cox17 exists in three almost equally populated redox states corresponding to $Cox17_{2S-S}$, $Cox17_{1S-S}$ and $Cox17_{0S-S}$, whereas in the Origami™(DE3) strain, $Cox17_{2S-S}$ is the prevalent redox form with only a minor amount of $Cox17_{3S-S}$ also present (Figure 3).

EXAFS sample of Cu_4Cox17

The sample preparation resulted in a copper concentration of 4.65 mM for the EXAFS sample of Cu_4Cox17. The ESI-MS spectra, presented in Figure 4, confirmed the presence of

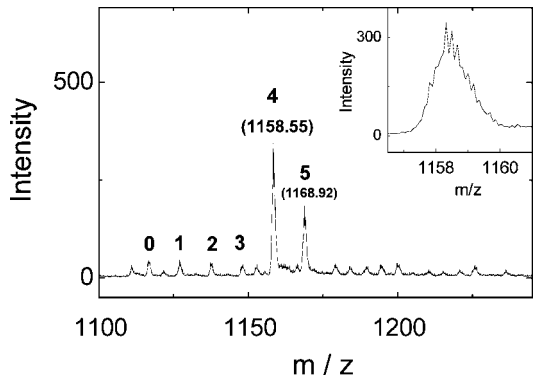

Figure 4 ESI-MS spectra of Cu_4Cox17 EXAFS sample

Spectra were measured at the following conditions: protein concentration 8 μM; 20 mM ammonium acetate, pH 7.5, 0.3 mM DTT, 25 °C. Charge state +6 ions are presented and numbers on the peaks denote the metal stoichiometry of the complex. Inset: fine structure of Cu_4Cox17 peaks.

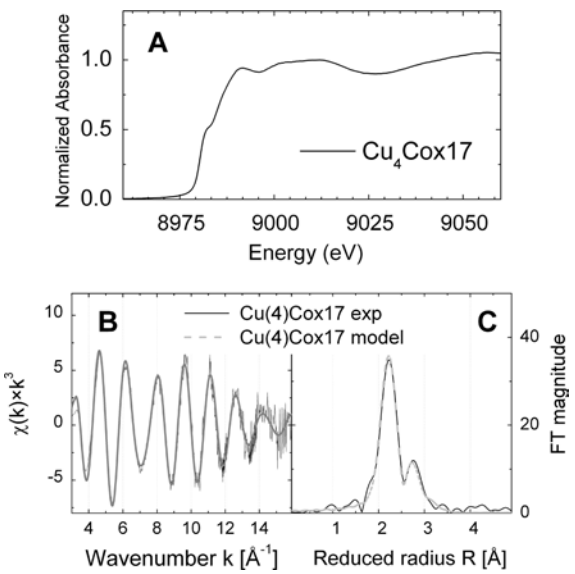

Figure 5 Characterization of metal-binding motif in Cu_4Cox17 by EXAFS

(**A**) Copper K-edge region in XANES spectrum of Cu_4Cox17. (**B**) $\mathbf{k}^3$-Weighted copper K-edge EXAFS spectrum and (**C**) corresponding Fourier-transformed spectrum. The continuous line shows the experimental data and the broken line shows the best fit.

Cu_4Cox17 as the major species in the sample. ESI–TOF MS investigation allows determination of masses with the precision of 5 p.p.m., which is sufficient for the quantification of disulfide bridges in the protein. The peak of the Cu_4Cox17 + 6 ion reveals the isotope resolution (Figure 4, inset) and the *m*/*z* value for the Cu_4Cox17 + 6 ion, at peak half-width, is 1158.58 Da.

X-ray absorption spectroscopy

Edge region

Figure 5(A) shows the K-edge region of the XAS spectrum for Cu_4Cox17 where the energy and shape of the edges are indicative of copper in the +1 oxidation state. An energy shift in the absorption edge was not observed during measurements, showing that the sample was stable in the beam and no radiation damage occurred. The spectrum of Cu_4Cox17 shows three absorptions at 8983.0 (inflection point from first derivative at 8982.7 eV), 8991.0 and 9000.0 eV, and a broad maximum at 9010.0 eV (Figure 5A).

Table 1 Cu-edge EXAFS fitting results for Cu_4Cox17

N, number of atoms; *R*, interatomic distance; σ^2, Debye-Waller parameter; E_F, Fermi energy; fit index: see definition in the Experimental section; R_{exafs}, R_{exafs}-factor (eqn 7). Values in parentheses represent the numerical precision (twice the S.D.) of the last digit. The Fermi energy E_F is related to the energetic position of the absorption edge (see Experimental section). The R_{exafs}-factor reflects the goodness of fit.

Fit strategy	Atom	*N*	*R* (Å)	σ^2 (Å^2)	E_F (eV)	Fit index, ε^2	R_{exafs} (%)
1	S	4	2.253 (4)	0.007 (1)	2 (0.6)	0.321	42.9
	Cu	1	2.90 (3)	0.005 (2)			
2	S	3	2.256 (2)	0.005 (1)	1 (0.4)	0.131	26.0
	Cu	1	2.72 (1)	0.006 (1)			
3	S	3	2.259 (2)	0.005 (1)	0.2 (0.4)	0.121	24.4
	Cu	2	2.71 (1)	0.007 (1)			
	Cu	1	2.87 (1)	0.007 (1)			

The absorption at 8982.7 eV is assigned to a 1s → 4p absorption that is typical for Cu^+ complexes. A number of studies have shown that the Cu^+ co-ordination number and/or geometry have influence on the intensity and sharpness of this transition, which decreases from linear bi-co-ordinated Cu^+ sites to tetrahedral ones [9,32–34]. In Cu_4Cox17, the 1s → 4p transition appears less intense and resolved than that observed in bi-co-ordinated Cu^+ sites [32,34] and is similar to the transition for trigonal model compounds [9,35], which indicates the presence of tri-co-ordinated Cu^+ centres in Cu_4Cox17. Furthermore, the K-edge region of the XAS spectrum for Cu_4Cox17 is strikingly similar to the corresponding spectra for Cu_4Ace1 (a copper-dependent gene-regulation factor) and Cu_4Ctr1C (the C-terminal domain of the yeast copper transporter Ctr1), which are two known copper proteins containing tetranuclear copper–thiolate clusters [25,26].

EXAFS region

The $\mathbf{k}^3$ weighted experimental EXAFS spectrum of Cu_4Cox17 and its Fourier-transformation are shown in Figures 5(B) and 5(C). The Fourier-transformed spectrum has two main peaks, indicating that the EXAFS arises from two prominent interactions (Figure 5C). The Fourier-transformed peak at 2.26 Å (1 Å = 0.1 nm) arises from the first shell ligand back-scattering and is indicative of the presence of sulfur atoms in the first co-ordination sphere of Cu^+. A copper–ligand distance of 2.26 Å is in the range of typical distances in trigonal Cu^+–thiolate complexes, which is 2.26– 2.28 Å, whereas distances in diagonal Cu–S complexes are approx. 2.16 Å [34]. The Fourier-transformed peak at 2.7 Å is characteristic for Cu–Cu interactions in polycopper–thiolate clusters and confirms its presence in Cu_4Cox17. To explore the structure of the cluster, different co-ordination numbers for sulfur and copper have been applied and the results of data refinement for Cu_4Cox17 are summarized in Table 1.

In a first model, four sulfur atoms at a distance of 2.25 Å and one copper atom at a distance of 2.90 Å were used to fit the data. It resulted in a poor simulation of the first peak in the Fourier-transformation and led to the conclusion that the number of sulfur atoms had to be diminished. In a second attempt, three sulfur atoms at a distance of 2.26 Å and one copper atom at a distance of 2.76 Å were used to fit the data. The first peak fitted well, but the amplitude of the second peak was not obtained. Taking the fit experience described above into account, and considering that the EXAFS and XANES of Cu_4Cox17 strongly resembles data published for Cu_4Ctr1C [25] and Cu_4Ace1 [26], a co-ordination similar to the one published in those papers is likely. Analysis of copper clusters in Cu_4Ctr1C and Cu_4Ace1 indicated the presence

of three Cu–S interactions at 2.25 Å and two different Cu–Cu interactions at 2.72 and 2.90 Å, with co-ordination numbers of 2 and 1 respectively. Both groups have shown that the Cu–Cu EXAFS from these two different copper interactions are nearly out of phase, and the resultant contribution at 2.7 Å is reduced substantially [25,26]. The EXAFS data for Cu_4Ctr1C and Cu_4Ace1 were collected up to $k = 13$ Å^{-1} [25,26], however, a longer energy range was available for the analysis of Cu_4Cox17 since this sample was zinc-free. By applying this fitting strategy to the Cu_4Cox17 data (fit strategy 3 in Table 1), a very good fit was obtained even when different starting values were used, and both copper–copper distances were jointly refined. This fitting result indicates that, in Cu_4Cox17, the average Cu^+ possess three Cu–S interactions at 2.26 Å and two different Cu–Cu interactions at 2.71 and 2.87 Å, with co-ordination numbers of 2 and 1. Corresponding theoretical curves, calculated from best fitting parameters, are presented in Figures 5(B) and 5(C).

The EXAFS sample of Cu_4Cox17 also contained a minor fraction of Cu_5Cox17 (Figure 4), whose occurrence has been observed previously [12]. Cu_5Cox17 may contain a cluster that is different from the Cu_4S_6 cage, and its presence may have an influence on the EXAFS results. It is reasonable to suggest that Cu_5Cox17 may contain Cu_5S_6-type clusters, which do exist in low-molecular-mass model systems and contain diagonally and trigonally co-ordinated metals [31]. To explore this possibility, we compared the Fourier-transformed spectra of Cu_4Cox17 with the Fourier-transformed spectra for Cu_4S_6 [30] and Cu_5S_6 [31] model clusters (Figure 6A), calculated from the spatial co-ordinates of model complexes from the Cambridge Structural Database. The comparison, illustrated in Figure 6(B), demonstrates close similarity of the Fourier-transformed spectrum for the Cu_4Cox17 sample to the spectrum of the Cu_4S_6 model cluster. Moreover, the presence of diagonal copper co-ordination should lead to a sharp peak in the rising edge of the XANES region. The absence of any indication of such a feature is fully consistent with these EXAFS results.

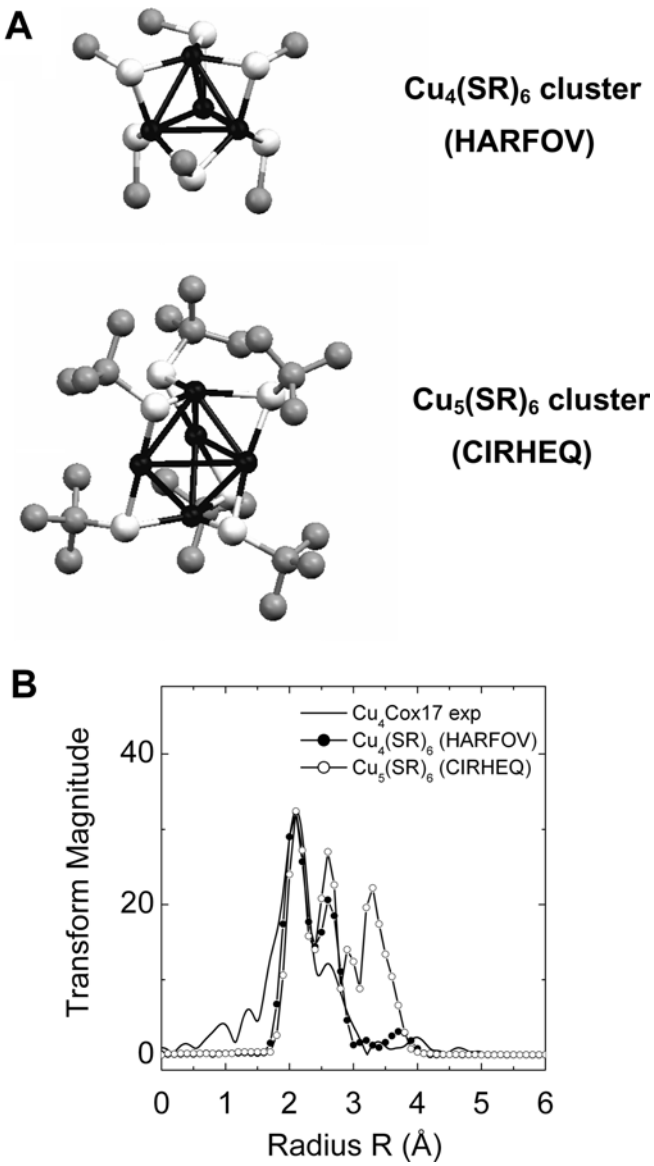

Figure 6 Comparision of Cu_4Cox17 with model clusters

(**A**) Structures of Cu_4S_6 (HARVOF) and Cu_5S_6 (CIRHEQ) model clusters. (**B**) Experimental Fourier-transformed EXAFS spectra for Cu_4Cox17 (continuous line) and theoretical spectra for Cu_4S_6 (●) and Cu_5S_6 (○) model clusters.

DISCUSSION

The results presented confirm the earlier finding that mammalian Cox17 can exist in three different redox states: fully reduced $Cox17_{0S\text{-}S}$, partially oxidized $Cox17_{2S\text{-}S}$ and fully oxidized $Cox17_{3S\text{-}S}$ [12], and shed light on the corresponding redox equilibria that are responsible for the interconversion of the various Cox17 states.

Equilibrium between $Cox17_{3S\text{-}S}$ and $Cox17_{2S\text{-}S}$

Reduction of $Cox17_{3S\text{-}S}$ to $Cox17_{2S\text{-}S}$ is fast and complete at millimolar concentrations of GSH, and the E_m between these Cox17 forms, as determined using GSH/GSSG redox buffers, is $E_{m1} = -197$ mV (pH 7.6, 37 °C). Localization of this labile disulfide bridge in $Cox17_{3S\text{-}S}$ could be derived from structural data available for yeast Cox17. Yeast apo-$Cox17_{2S\text{-}S}$ contains two C-terminal helixes interlinked by two disulfide bonds, Cys^{26}–Cys^{57} and Cys^{36}–Cys^{47}, whereas two vicinal residues, Cys^{23} and Cys^{24}, are reduced [11]. Mammalian Cox17 might have a similar disulfide bond array in apo-$Cox17_{2S\text{-}S}$ and therefore an E_{m1} of -197 mV could be ascribed to the redox equilibrium between the two vicinal Cys^{22} and Cys^{23} in human apo-$Cox17_{2S\text{-}S}$.

As the cellular redox potential is much more negative (values are presented below), the result obtained indicates that it is most likely that fully oxidized $Cox17_{3S\text{-}S}$ does not exist under cellular conditions. In the presence of GSSG, however, there is a GSH–$Cox17_{2S\text{-}S}$ adduct observed in MS spectra. The ability of Cox17 to form mixed disulfide adducts with GSH as well as with 2-mercaptoethanol is known [19]. The present results demonstrate that the amount of GSH–$Cox17_{2S\text{-}S}$ adduct depends on the redox potential of the environment and forms a bell-shaped curve with a maximum around the E_m of $Cox17_{3S\text{-}S}$ (Figure 1A).

Many proteins form protein disulfide adducts with GSH under both *in vitro* and *in vivo* conditions, and protein glutathionylation is supposed to have various physiological consequences. S-glutathionylation, occurring during oxidative and nitrosative stress, protects critical cysteine residues against irreversible oxidation to sulfinic and sulfonic acids and enhances cellular resistance to oxidative and nitrosative stress (reviewed in [36]). Moreover, protein glutathionylation occurring during NO-dependent signal-transduction modulates many key proteins such as tyrosine kinases, and is part of signal transduction [37]. There also are suggestions that protein glutathionylation affects

proteolytic processing, ubiquitination and degradation of some proteins [38].

Glutathionylation of $Cox17_{2S\text{-}S}$ might alter metal-binding properties of Cox17 and regulate its functioning as a copper chaperone. Earlier, we demonstrated that the GSH–$Cox17_{2S\text{-}S}$ adduct cannot bind Cu^+, which is critical for functioning of Cox17 as a copper chaperone [19]. Decomposition of GSH–$Cox17_{2S\text{-}S}$ adducts with DTT restored the copper-binding ability of $Cox17_{2S\text{-}S}$, demonstrating that Cox17 could be reversibly regulated with GSH [19]. Current results demonstrate that the presence of oxidized GSSG promotes formation of GSH–$Cox17_{2S\text{-}S}$ adducts and, therefore, it is not excluded that this adduct could form in oxidative stress conditions by the action of cellular GSSG, where the concentration may reach millimolar levels.

Equilibrium between $Cox17_{2S\text{-}S}$ and $Cox17_{0S\text{-}S}$

Thermodynamically and kinetically, reduction of disulfide bonds in $Cox17_{2S\text{-}S}$ is much more difficult than reduction of the first disulfide bond in $Cox17_{3S\text{-}S}$. Even by the action of a high concentration of DTT (5 mM) and an elevated temperature (37 °C), reduction occurs with a half-life of 20 min (Figure 2). Both disulfide bonds are reduced simultaneously, as intermediates of Cox17 with one disulfide bond were not observed. The activation energy for the reduction of $Cox17_{2S\text{-}S}$ by DTT is −60 kJ/mol, which is characteristic for typical chemical reactions that obey van't Hoff's rule. The result obtained suggests that the conformational changes in the rigid structure of $Cox17_{2S\text{-}S}$ are apparently not rate-limiting and reduction might be limited by the restricted accessibility of disulfides in $Cox17_{2S\text{-}S}$ by the reducing agent. The E_m between $Cox17_{2S\text{-}S}$ and $Cox17_{0S\text{-}S}$, determined by using the DTT/DTT_{ox} redox buffers, was $E_{m2} = -340$ mV (pH 7.6, 37 °C).

The importance of the intracellular redox potential for cellular functioning has been recognized for a long time; however, methods for its correct determination have only been discovered recently. Initially, the cellular redox potential of cytosol was calculated to be in the range of −200 to −240 mV. These values arose from analytically determined cellular concentrations of GSH and GSSG alone, and therefore other cellular redox couples were not taken into account [21]. During the last decade, a number of more reliable approaches have been developed, which enable *in situ* determination of cellular redox potential. These methods make use of redox-sensitive molecular probes [39] or recombinant proteins, especially GFP, which can be targeted to different cellular compartments [16–18]. The results obtained demonstrate that the cellular redox environment is highly reducing, and redox potential in the cytoplasm and mitochondrial matrix of mammalian and plant cells is characterized by redox potential values of approx. −320 mV (pH 7.0, 25–30 °C) and −360 mV (pH 7.8, 37 °C) [16–18] respectively.

The E_m of $Cox17_{2S\text{-}S}$ is −305 mV (recalculated for pH 7.0, 25 °C), close to that of the cytoplasmic redox potential of −320 mV (pH 7.0, 25 °C) [18], which suggests that there exists an equilibrium between the fully reduced $Cox17_{0S\text{-}S}$ and partially oxidized $Cox17_{2S\text{-}S}$ in the cytosol. To test this assumption, we have determined the oxidative status of overexpressed Cox17 in the cytosol of two *E. coli* strains carrying the expression plasmid containing the Cox17 insert. In the BL21pLysS(DE3) strain, we observed the presence of the fully reduced $Cox17_{0S\text{-}S}$ and the partially oxidized $Cox17_{2S\text{-}S}$ (Figure 3A). In *E. coli* Origami™(DE3) strain, which is characterized by a more oxidative cellular redox potential [40], Cox17 was present solely in the partially oxidized $Cox17_{2S\text{-}S}$ form (Figure 3B). The results obtained from these bacteria demonstrate the presence of the partially oxidized $Cox17_{2S\text{-}S}$ in bacterial cytosol, which suggests that the redox potential in the bacterial cytosol might be similar to that in mammalian cells. The presence of the partially oxidized $Cox17_{2S\text{-}S}$ form, at more oxidative but still tolerable redox potentials, demonstrates that $Cox17_{2S\text{-}S}$ might be the predominant redox form of Cox17 in more oxidative conditions, which also exist in the IMS.

Structure of the metal-binding motifs in Cu_4Cox17

Luminescence and MS evidence of Cu_4Cox17 point to the presence of a polymetal–thiolate cluster in mammalian Cu_4Cox17 [12]; however, the metal-binding motif in Cu_4Cox17 has not been structurally characterized. Cox17 has complicated metal-binding and redox properties and sample preparation plays a crucial role in its structural studies. In the present study, we have succeeded in preparing a well-defined sample of Cu_4Cox17 suitable for structural studies by EXAFS. ESI-MS and XANES analysis of the sample confirmed that the protein is the fully reduced major metalloform Cu_4Cox17, and copper ions are bound in the form of Cu^+. According to the EXAFS results, copper atoms in Cu_4Cox17 are part of a cluster and are co-ordinated by three sulfur atoms, which suggests that the metal-binding motif in Cu_4Cox17 could be modelled by well-known Cu_4S_6-type model clusters [30,41] depicted in Figure 6(A). This model implies that all six cysteine residues of Cox17 participate in the cluster formation. Alignment of Cox17 sequences from evolutionally distant organisms, such as yeast (*Saccharomyces cerevisiae*), green algae (*Chlamydomonas reinhardtii*), *Plasmodium yoelii yoelii*, plants (*Arabidopsis thaliana*) and humans, demonstrates that there are six absolutely conserved cysteine residues in Cox17 (Figure 7B), which is in agreement with the suggested model (Figure 7A) and allows us to conclude that the functional role for six conserved cysteine residues in Cox17 might be connected with the formation of a Cu_4S_6-type of copper–thiolate cluster.

There are indications that the metal cluster in Cu_4Cox17 differs slightly from the ideal Cu_4S_6-type cluster, characterized by three equal Cu–Cu distances of 2.70 Å. The EXAFS analysis of Cu_4Cox17 shows two short Cu–Cu distances of 2.71 Å and one long Cu–Cu distance of 2.87 Å (see Table 1). Besides Cox17, there are two other proteins known to contain Cu_4S_6-type clusters. They are the copper-dependent gene regulation factor, Ace1, and the C-terminal domain of the yeast copper transporter, Ctr1C. EXAFS analysis of tetracopper clusters in both Ace1 [26] and Ctr1C [25] demonstrated the presence of two short and one long Cu–Cu distance, which is similar to our result for Cu_4Cox17. Taken together, it is not excluded that in proteins it is difficult to achieve ideal Cu_4S_6-type cages, which are always more or less distorted.

The ESI-MS analysis demonstrates that the Cu_4Cox17 metalloform could not be prepared in homogeneous form, since Cu_4Cox17 is always accompanied by a minor Cu_5Cox17 metalloform, which is in a dynamic equilibrium with Cu_4Cox17 [12]. The structure of the Cu_5Cox17 form is currently unknown; however, EXAFS analysis in the present study indicates that, most probably, Cu_5Cox17 does not contain a Cu_5S_6-type cluster. The composition and spatial structure of Cu_5Cox17 as well as of Cu_4Cox17 forms remains to be established; however, the presence of a dynamic equilibrium in the sample may seriously complicate structural studies of these metalloforms. Moreover, we have evidence from size-exclusion chromatography that porcine Cu_4Cox17 has a tendency for oligomerization at higher protein concentrations, similar to the highly copper-loaded forms of yeast CuCox17 [10], which further complicates structural studies of mammalian Cu_4Cox17.

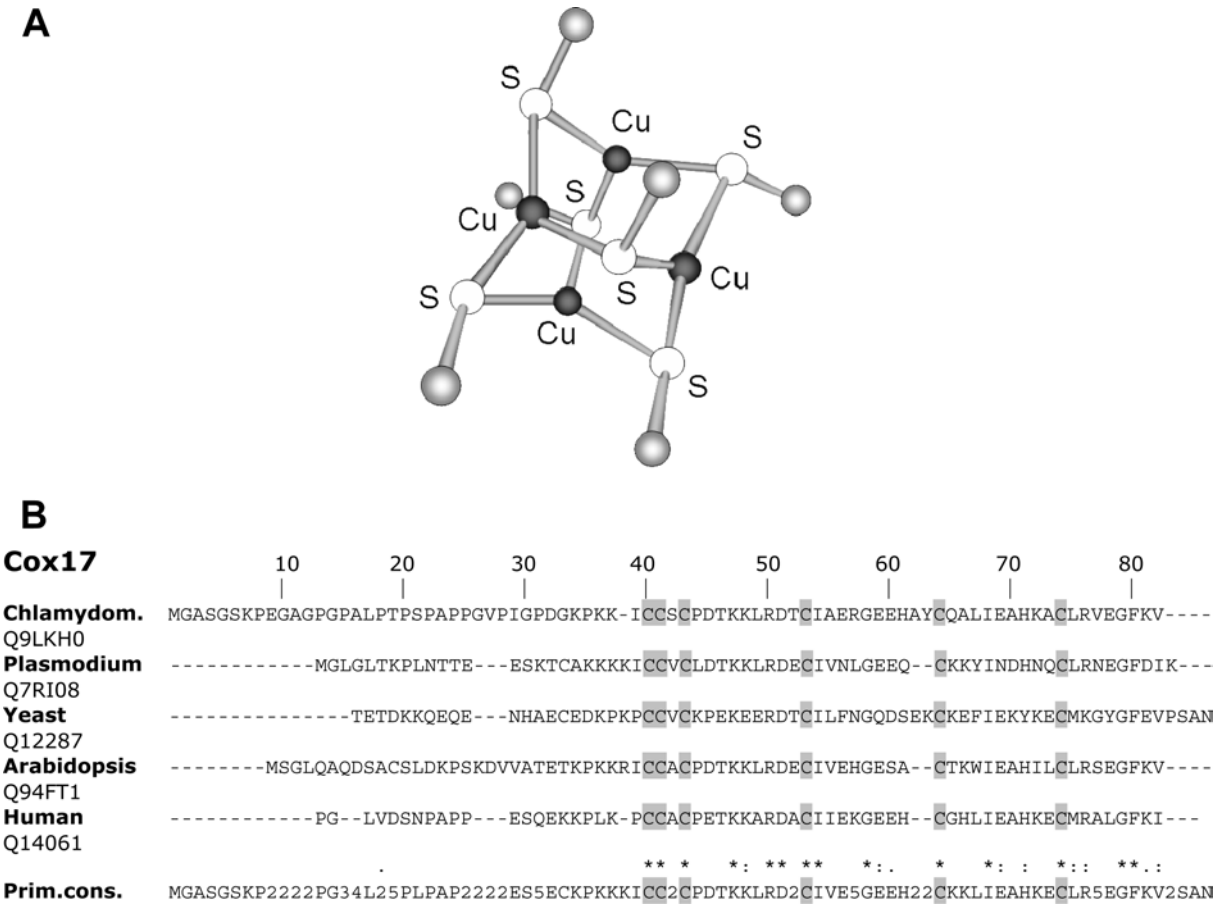

Figure 7 Proposed structure of the metal-binding motif in Cu_4Cox17 and alignment of Cox17 sequences

(**A**) Structure of the $Cu_4(S)_6$ model cluster proposed for the copper–thiolate cluster in Cu_4Cox17. (**B**) Sequence alignment of Cox17 from yeast (*Saccharomyces cerevisiae*), green alga (Chlamydom.; *Chalymodomonas reinhardtii*), *Plasmodium yoelii yoelii*, plant (*Arabidopsis thaliana*) and humans. Prim. cons., primary consensus sequence; *, identity; :, conservative replacement; ., non-conservative replacement.

Comparing our results for mammalian Cox17 with available data for yeast Cox17 we can conclude that both proteins can form low-stoichiometry and high-stoichiometry metalloforms. Low-stoichiometry metalloforms of yeast $Cu_1Cox17_{2S\text{-}S}$ are structurally characterized and the copper ion is diagonally co-ordinated by two cysteine residues [11]. It is realistic that the high-stoichiometry metalloforms of yeast Cox17 are similar to the mammalian Cox17, which could be confirmed by structural studies with well-characterized samples of yeast CuCox17.

Biological context

Cox17 has a double cellular localization as it is distributed in the cytosol and in the IMS [42]. Recently, it was demonstrated that many proteins, including Cox17, which do not contain mitochondrial targeting sequences, have a special oxidative mechanism of transport into the IMS [43]. This mechanism operates only for fully reduced proteins, which enter into the IMS through mitochondrial outer membrane pores and are oxidized by oxidized Mia40 proteins, which is crucial for their retention in the IMS [15]. Such an oxidative folding, with the involvement of four cysteine residues in imported proteins, has been demonstrated to operate not only for Cox17 but also for other proteins containing twin Cys-Xaa_9-Cys motifs (Mia 40, Cox19 and Cox23) or twin Cys-Xaa_3-Cys motifs (the small Tim proteins Tim8, Tim9, Tim10 and Tim13) [43]. All of these proteins should therefore have similar redox properties and, indeed, the recently determined E_m for Tim10 of -320 mV (pH 7.4, 25 °C) [44] is very similar to the E_m of $Cox17_{2S\text{-}S}$, thus supporting the theory of a similar oxidative transport mechanism. There is no information about the E' in the IMS; however, it is reasonable to assume that it is more oxidative, as compared with the cytosol. In addition to excessive oxidation by-products, the IMS has a lower pH (pH 6.88) as compared with the pH in the cytosol (pH 7.6) [45], which alone lowers the redox potential of the IMS environment to less than -300 mV. On the basis of these considerations, $Cox17_{2S\text{-}S}$ might be the predominate redox form of Cox17 in the IMS.

It is possible that *de novo* synthesized Cox17 may be partially oxidized to $Cox17_{2S\text{-}S}$ in the cellular cytosol before being transported into the IMS. A similar situation was discussed in the case of Tim 10, partial oxidation of which has been demonstrated to prevent its transport into the IMS [44]. As binding of Zn^{2+} slowed down the oxidation of Tim10, and the Zn(II)–Tim10 complex was able to enter into the IMS, it was suggested that binding of Zn^{2+} might be essential to maintain the Tim10 protein in a reduced and import-competent state in the cytosol [44]. A similar mechanism may also occur in the case of Cox17, as fully reduced $Cox17_{0S\text{-}S}$ can bind up to two Zn^{2+} [12]. Moreover, these current results demonstrate that micromolar concentrations of Zn^{2+} have a strong inhibitory effect on the air oxidation of $Cox17_{0S\text{-}S}$. Fully reduced Cox17 might also bind to four Cu^+ to form a Cu_4Cox17 complex [12], which is most likely to

be retained in the cytosol, as mitochondrial outer membrane pores are not permeable to copper-loaded protein complexes [46].

Cox17 participates in the delivery of copper to CCO in yeast and in mammalian cells; however, at least five other proteins, Cox11, Sco1, Sco2, Cox19 and Cox23, are involved in this process [3]. Experiments with yeast demonstrate that yeast Cox17 transfers Cu^+ to Cox11 and Sco1 proteins [47]. Metal-transfer experiments with human $Cu_1Cox17_{2S\text{-}S}$ and human Sco1 demonstrate that $Cu_1Cox17_{2S\text{-}S}$ forms a specific metal-bridged protein–protein complex with Sco1 [13], indicating that $Cox17_{2S\text{-}S}$ is the biologically active form, which transfers metals to the Sco1 protein. Apparently, oxidative transport of Cox17 into the IMS is important not only for retention of $Cox17_{2S\text{-}S}$ in the IMS but also for formation of its biologically competent form.

In contrast with $Cu_1Cox17_{2S\text{-}S}$, the biological role of Cu_4Cox17 is currently not clear. On the basis of our results, Cu_4Cox17 predominantly exists in the cellular cytosol, which is characterized by a more reducing environment, as compared with the IMS. Highly copper-loaded Cox17 has been shown to exist under excess copper conditions in yeast and mammalian cells, and these forms might be involved in storage of Cu^+ [11]. Polycopper–thiolate clusters, similar to the tetracopper–thiolate cluster in Cu_4Cox17, are known to exist in copper-substituted metallothioneins (MTs), which are low-molecular-mass cysteine-rich proteins involved in metabolism of biometals such as zinc and copper and toxic metals such as cadmium [48]. There is a consensus of opinion that copper–thiolate clusters of MTs participate in storage and detoxification of potentially toxic copper ions by redox silencing, which suppresses the copper-catalysed production of free radicals and has an antioxidative effect [49]. By analogy with MTs, the polycopper–thiolate clusters in Cu_4Cox17 might also be involved in redox silencing of copper ions and also have antioxidative properties. Interestingly, expression of the plant Cox17 gene is induced in conditions of oxidative stress, which suggests that, at least in plants, Cox17, in addition to its primary role as copper chaperone, may also act as antioxidative protein [50].

In mammals, Cox17 may also have additional functions. In mice, the levels of Cox17 mRNA are elevated in endocrine and neuroendocrine cells, whereas the highest levels of Cox17 mRNA in brain were found in pituitary glands [42]. These endocrine cells contain PAMO (peptidylglycine α-amidating mono-oxygenase) and dopamine β-hydroxylase, which are polycopper oxidases, which amidate the C-terminus of neuropeptides/peptide hormones and convert dopamine into noradrenaline respectively. Both copper enzymes are localized in perinuclear regions, such as the endoplasmatic reticulum and the Golgi. Interestingly, in mouse AtT-20 (pituitary epithelial-like tumour) cell lines, which are rich in perinuclear PAMO, Cox17 was localized in the perinuclear region, which strongly suggests that mammalian Cox17 could also be involved in the delivery of copper to perinuclear polycopper oxidases such as PAMO and dopamine β-hydroxylase [42]. Copper transfer to polycopper oxidases could be mediated by Cu_4Cox17, which can donate multiple copper ions to a partner protein.

Based on our results, Figure 8 illustrates the process of oxidative switching of mammalian Cox17. The major oxidative switch occurs in the IMS after the transport of the fully reduced $Cox17_{0S\text{-}S}$ into the IMS. Once in the IMS, Mia40 mediates the switch to its biologically active form, $Cox17_{2S\text{-}S}$. The second oxidative switch converts $Cox17_{2S\text{-}S}$ into the fully oxidized protein $Cox17_{3S\text{-}S}$ or GSH–$Cox17_{2S\text{-}S}$, which inhibits metal binding. This switch is relatively minor as it may only occur in conditions of high oxidative stress.

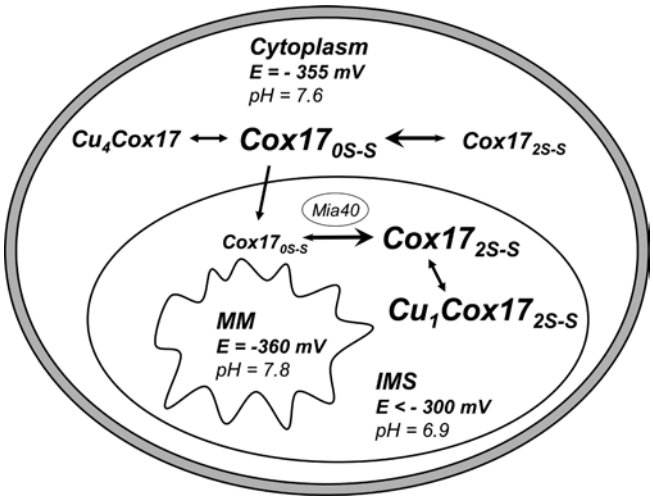

Figure 8 Schematic representation of Cox17 redox equilibria in the different cellular compartments

pH-corrected redox potentials (E) in cytosol and MM were calculated from the corresponding experimental values $E = -320$ mV (pH 7.0) [18] and $E = -360$ mV (pH 7.8) [16]. pH values in cytosol, IMS and MM were taken from [45]. E_m values for the $Cox17_{2S\text{-}S} \leftrightarrow Cox17_{0S\text{-}S}$ couple in the cytosol and the IMS are -340 mV (pH 7.6) and -300 mV (pH 6.9) respectively.

These oxidative switches may be passively regulated by the redox potential of the environment. However, as each oxidative state of the Cox17 protein involves a separate and biologically important function, it is no surprise that its regulation may be mediated by other specific factors, such as Mia40. Moreover, complexation of $Cox17_{0S\text{-}S}$ with Zn^{2+} in the cytosol might inhibit oxidation of $Cox17_{0S\text{-}S}$ until its transport into the IMS, whereas co-operative binding of four copper ions leads to the formation of tetracopper-hexathiolate clusters. Highly copper-loaded forms of Cox17 might be involved in the storage and/or transfer of Cu^+ to polycopper oxidases in specialized mammalian cells.

This work was supported by the Estonian Science Foundation project 7191, the EU (European Union) 5th Framework Project 02435, Karolinska Institutet, the EU-I3 access grant from the EC (Enzyme Commission) - Research Infrastructure Action under the FP6 'Structuring the European Research Area Program' and the Deutsche Forschungsgemeinschaft.

REFERENCES

1 Ferguson-Miller, S. and Babcock, G. T. (1996) Heme/copper terminal oxidases. Chem. Rev. **96**, 2889–2908
2 Tsukihara, T., Aoyama, H., Yamashita, E., Tomizaki, T., Yamaguchi, H., Shinzawa-Itoh, K., Nakashima, R., Yaono, R. and Yoshikawa, S. (1996) The whole structure of the 13-subunit oxidized cytochrome-*c* oxidase at 2.8 Å. Science **272**, 1136–1144
3 Cobine, P. A., Pierrel, F. and Winge, D. R. (2006) Copper trafficking to the mitochondrion and assembly of copper metalloenzymes. Biochim. Biophys. Acta **1763**, 759–772
4 Glerum, D. M., Shtanko, A. and Tzagoloff, A. (1996) SCO1 and SCO2 act as high copy suppressors of a mitochondrial copper recruitment defect in *Saccharomyces cerevisiae*. J. Biol. Chem. **271**, 20531–20535
5 Punter, F. A. and Glerum, D. M. (2003) Mutagenesis reveals a specific role for Cox17p in copper transport to cytochrome oxidase. J. Biol. Chem. **278**, 30875–30880
6 Carr, H. S. and Winge, D. R. (2003) Assembly of cytochrome-*c* oxidase within the mitochondrion. Acc. Chem. Res. **36**, 309–316
7 Glerum, D. M., Shtanko, A. and Tzagoloff, A. (1996) Characterization of COX17, a yeast gene involved in copper metabolism and assembly of cytochrome oxidase. J. Biol. Chem. **271**, 14504–14509
8 Takahashi, Y., Kako, K., Kashiwabara, S., Takehara, A., Inada, Y., Arai, H., Nakada, K., Kodama, H., Hayashi, J., Baba, T. and Munekata, E. (2002) Mammalian copper chaperone Cox17p has an essential role in activation of cytochrome-*c* oxidase and embryonic development. Mol. Cell. Biol. **22**, 7614–7621

9 Srinivasan, C., Posewitz, M. C., George, G. N. and Winge, D. R. (1998) Characterization of the copper chaperone Cox17 of *Saccharomyces cerevisiae*. Biochemistry **37**, 7572–7577

10 Heaton, D. N., George, G. N., Garrison, G. and Winge, D. R. (2001) The mitochondrial copper metallochaperone Cox17 exists as an oligomeric, polycopper complex. Biochemistry **40**, 743–751

11 Arnesano, F., Balatri, E., Banci, L., Bertini, I. and Winge, D. R. (2005) Folding studies of Cox17 reveal an important interplay of cysteine oxidation and copper binding. Structure **13**, 713–722

12 Palumaa, P., Kangur, L., Voronova, A. and Sillard, R. (2004) Mechanism of metal binding by Cox17, a copper chaperone for cytochrome-*c* oxidase. Biochem. J. **382**, 1–8

13 Banci, L., Bertini, I., Ciofi-Baffoni, S., Leontari, I., Martinelli, M., Palumaa, P., Sillard, R. and Wang, S. (2007) Human Sco1 functional studies and pathological implications of the P174L mutant. Proc. Natl. Acad. Sci. U.S.A. **104**, 15–20

14 Chacinska, A., Pfannschmidt, S., Wiedemann, N., Kozjak, V., Sanjuan Szklarz, L. K., Schulze-Specking, A., Truscott, K. N., Guiard, B., Meisinger, C. and Pfanner, N. (2004) Essential role of Mia40 in import and assembly of mitochondrial intermembrane space proteins. EMBO J. **23**, 3735–3746

15 Mesecke, N., Terziyska, N., Kozany, C., Baumann, F., Neupert, W., Hell, K. and Herrmann, J. M. (2005) A disulfide relay system in the intermembrane space of mitochondria that mediates protein import. Cell **121**, 1059–1069

16 Hanson, G. T., Aggeler, R., Oglesbee, D., Cannon, M., Capaldi, R. A., Tsien, R. Y. and Remington, S. J. (2004) Investigating mitochondrial redox potential with redox-sensitive green fluorescent protein indicators. J. Biol. Chem. **279**, 13044–13053

17 Jiang, K., Schwarzer, C., Lally, E., Zhang, S., Ruzin, S., Machen, T., Remington, S. J. and Feldman, L. (2006) Expression and characterization of a redox-sensing green fluorescent protein (reduction-oxidation-sensitive green fluorescent protein) in *Arabidopsis*. Plant Physiol. **141**, 397–403

18 Dooley, C. T., Dore, T. M., Hanson, G. T., Jackson, W. C., Remington, S. J. and Tsien, R. Y. (2004) Imaging dynamic redox changes in mammalian cells with green fluorescent protein indicators. J. Biol. Chem. **279**, 22284–22293

19 Voronova, A., Kazantseva, J., Tuuling, M., Sokolova, N., Sillard, R. and Palumaa, P. (2007) Cox17, a copper chaperone for cytochrome-*c* oxidase: expression, purification, and formation of mixed disulphide adducts with thiol reagents. Protein Expression Purif. **53**, 138–144

20 Cleland, W. W. (1964) Dithiothreitol, a new protective reagent for SH groups. Biochemistry **3**, 480–482

21 Schafer, F. Q. and Buettner, G. R. (2001) Redox environment of the cell as viewed through the redox state of the glutathione disulfide/glutathione couple. Free Radicals Biol. Med. **30**, 1191–1212

22 Szajewski, R. P. and Whitesides, G. M. (1980) Rate constants and equilibrium constants for thiol–disulfide interchange reactions involving oxidized glutathione. J. Am. Chem. Soc. **102**, 2011–2016

23 Pettifer, R. F. and Hermes, C. J. (1985) Absolute energy calibration of X-ray radiation from synchrotron sources. J. Appl. Crystallogr. **18**, 404–412

24 Cramer, S. P., Tench, O., Yocum, M. and George, G. N. (1988) A 13-element Ge detector for fluorescence EXAFS. Nucl. Instrum. Methods Phys. Res. Sect. A **266**, 586–591

25 Xiao, Z., Loughlin, F., George, G. N., Howlett, G. J. and Wedd, A. G. (2004) C-terminal domain of the membrane copper transporter Ctr1 from *Saccharomyces cerevisiae* binds four Cu(I) ions as a cuprous–thiolate polynuclear cluster: sub-femtomolar Cu(I) affinity of three proteins involved in copper trafficking. J. Am. Chem. Soc. **126**, 3081–3090

26 Brown, K. R., Keller, G. L., Pickering, I. J., Harris, H. H., George, G. N. and Winge, D. R. (2002) Structures of the cuprous–thiolate clusters of the Mac1 and Ace1 transcriptional activators. Biochemistry **41**, 6469–6476

27 Reference deleted

28 Lippold, B., Meyer-Klaucke, W., Meyer, T. and Henkel, G. (2005) Towards an automated quality control of XAS data. J. Synchrotron Radiat. **12**, 45–52

29 Reference deleted

30 Baumgartner, M., Schmalle, H. and Baerlocher, C. (1993) Synthesis, characterization, and crystal structure of three homoleptic copper(I) thiolates: $[Cu(CH_3S^-)]$, $[(C_6H_5)_4P^+]_2[Cu_5(CH_3S^-)_7].C_2H_6O_2$, and $[(C_3H_7)_4N^+]_2[Cu_4(CH_3S^-)_6].CH_4O$. J. Solid State Chem. **107**, 63–75

31 Bowmaker, G. A., Clark, G. R., Seadon, J. K. and Dance, I. G. (1984) The formation and structural chemistry of the hexa(-tert-butylthiolato)pentacuprate(I) cage anion with triethylammonium and tetraethylammonium cations. Polyhedron **3**, 535–544

32 Ralle, M., Cooper, M. J., Lutsenko, S. and Blackburn, N. J. (1998) The Menkes disease protein binds copper via novel 2-coordinate Cu(I)-cysteinates in the N-terminal domain. J. Am. Chem. Soc. **120**, 13525–13526

33 DiDonato, M., Hsu, H. F., Narindrasorasak, S., Que, L. J. and Sarkar, B. (2000) Copper-induced conformational changes in the N-terminal domain of the Wilson disease copper-transporting ATPase. Biochemistry **39**, 1890–1896

34 Gnida, M., Ferner, R., Gremer, L., Meyer, O. and Meyer-Klaucke, W. (2003) A novel binuclear [CuSMo] cluster at the active site of carbon monoxide dehydrogenase: characterization by X-ray absorption spectroscopy. Biochemistry **42**, 222–230

35 Eisses, J. F., Stasser, J. P., Ralle, M., Kaplan, J. H. and Blackburn, N. J. (2000) Domains I and III of the human copper chaperone for superoxide dismutase interact via a cysteine-bridged dicopper(I) cluster. Biochemistry **39**, 7337–7342

36 Biswas, S., Chida, A. S. and Rahman, I. (2006) Redox modifications of protein–thiols: emerging roles in cell signaling. Biochem. Pharmacol. **71**, 551–564

37 Barrett, W. C., DeGnore, J. P., Konig, S., Fales, H. M., Keng, Y. F., Zhang, Z. Y., Yim, M. B. and Chock, P. B. (1999) Regulation of PTP1B via glutathionylation of the active site cysteine 215. Biochemistry **38**, 6699–66705

38 Obin, M., Shang, F., Gong, X., Handelman, G., Blumberg, J. and Taylor, A. (1998) Redox regulation of ubiquitin-conjugating enzymes: mechanistic insights using the thiol-specific oxidant diamide. FASEB J. **12**, 561–569

39 Bernhardt, P. V., Chen, K. I. and Sharpe, P. C. (2006) Transition metal complexes as mediator-titrants in protein redox potentiometry. J. Biol. Inorg. Chem. **11**, 930–936

40 Bessette, P. H., Aslund, F., Beckwith, J. and Georgiou, G. (1999) Efficient folding of proteins with multiple disulfide bonds in the *Escherichia coli* cytoplasm. Proc. Natl. Acad. Sci. U.S.A. **96**, 13703–13708

41 Coucouvanis, D., Murray, C. N. and Kanodia, S. K. (1980) Metal-mercaptide chemistry. Synthesis and structural characterization of the $[Cu(SC_6H_5)]^{2-}$ anion. Rational synthesis and the structure of the $[Cu_4(SC_6H_5)_6]$ cluster. Inorg. Chem. **19**, 2993–2998

42 Kako, K., Tsumori, K., Ohmasa, Y., Takahashi, Y. and Munekata, E. (2000) The expression of Cox17p in rodent tissues and cells. Eur. J. Biochem. **267**, 6699–6707

43 Herrmann, J. M. and Kohl, R. (2007) Catch me if you can! Oxidative protein trapping in the intermembrane space of mitochondria. J. Cell. Biol. **176**, 559–563

44 Lu, H. and Woodburn, J. (2005) Zinc binding stabilizes mitochondrial Tim10 in a reduced and import-competent state kinetically. J. Mol. Biol. **353**, 897–910

45 Porcelli, A. M., Ghelli, A., Zanna, C., Pinton, P., Rizzuto, R. and Rugolo, M. (2005) pH difference across the outer mitochondrial membrane measured with a green fluorescent protein mutant. Biochem. Biophys. Res. Commun. **326**, 799–804

46 Chen, W. J. and Douglas, M. G. (1987) The role of protein structure in the mitochondrial import pathway. Unfolding of mitochondrially bound precursors is required for membrane translocation. J. Biol. Chem. **262**, 15605–15609

47 Horng, Y. C., Cobine, P. A., Maxfield, A. B., Carr, H. S. and Winge, D. R. (2004) Specific copper transfer from the Cox17 metallochaperone to both Sco1 and Cox11 in the assembly of yeast cytochrome-*c* oxidase. J. Biol. Chem. **279**, 35334–35340

48 Vasak, M. and Kägi, J. H. R. (1994) Metallothioneins. In Encyclopedia of Inorganic Chemistry (King, R. B., ed.), pp. 2229–2241, J. Wiley & Sons Ltd, New York

49 Tapiero, H., Townsend, D. M. and Tew, K. D. (2003) Trace elements in human physiology and pathology: copper. Biomed. Pharmacother. **57**, 386–98

50 Balandin, T. and Castresana, C. (2002) AtCOX17, an *Arabidopsis* homolog of the yeast copper chaperone COX17. Plant Physiol. **129**, 1852–1857

Received 15 June 2007/1 August 2007; accepted 2 August 2007
Published as BJ Immediate Publication 2 August 2007, doi:10.1042/BJ20070804